Journal of Solid State Chemistry **154,** 466–475 (2000)
doi:10.1006/jssc.2000.8866, available online at http://www.idealibrary.com on IDEAL®

High-Pressure Tungsten Bronzes, RE_xWO_3 with RE = La and Nd, Studied by X-Ray Diffraction and Electron Microscopy

C. Grenthe,* M. Sundberg,* V. P. Filonenko,† and I. P. Zibrov‡

*Department of Inorganic Chemistry, Arrhenius Laboratory, Stockholm University, S-106 91 Stockholm, Sweden; †Institute for High Pressure Physics, Russian Academy of Sciences, Troitsk, 142190 Moscow region, Russia; and ‡Institute of Crystallography, Russian Academy of Sciences, 117 333 Moscow, Russia

E-mail: marsu@inorg.su.se

Received March 27, 2000; in revised form June 14, 2000; accepted July 13, 2000; published online August 30, 2000

Rare earth tungsten bronzes, $La_{0.1}WO_3$ and Nd_xWO_3 with $x = 0.1$ and 0.2, have been prepared by solid state reaction at $P = 30$ kbar and $T = 1320–1620$ K and structurally characterized by X-ray diffraction and electron microscopy. The hexagonal tungsten bronze (HTB) structure was found in all samples, whereas intergrowth tungsten bronzes of (n)-ITB and $(1, n)$-ITB structure types have only been observed in samples prepared at $T > 1500$ K. The ITB structures can be considered as an intergrowth of slabs of WO_3-type, n octahedra wide, and slices of HTB-type. In the (n)-ITB family the slices of HTB-type are one hexagonal tunnel row wide, whereas they are two hexagonal tunnel rows wide in the $(1, n)$-ITB phases. Members of the (n)-ITB family were frequently observed in the high-temperature samples. The La_xWO_3 bronzes, (2)-ITB, (3)-ITB, (1, 2)-ITB, and HTB, are new. In the Nd_xWO_3 system a perovskite tungsten bronze (PTB) of composition $Nd_{\approx 0.1}WO_3$ and a (3)-ITB bronze were found in addition to the previously reported high-pressure phases (2)-ITB and HTB. The bronze structures were well-ordered, but a few exceptions were observed. A couple of defects are described along with proposed defect models. Microanalyses show that the hexagonal tunnel sites in the ITB and HTB structures are less than half-filled with RE atoms. The relationships between the RE_xWO_3 bronzes and the alkali tungsten bronzes, A_xWO_3, are discussed. © 2000 Academic Press

INTRODUCTION

Recent investigations of the ternary systems Nd–W–O and Pr–W–O have shown the existence of several new phases of alkali tungsten bronze type in samples prepared by solid state reaction at high pressure ($P = 50$ kbar) and temperatures of $T = 1520–1570$ K (1,2). In the first system both ordered and disordered crystals of the intergrowth tungsten bronze (2)-ITB and of hexagonal tungsten bronze (HTB) have been identified from their electron diffraction patterns and high-resolution transmission electron microscopy (HRTEM) images. The (2)-ITB structure can be described as an ordered intergrowth of slices of HTB-type, one hexagonal tunnel row wide and WO_3-slabs, two WO_6-octahedra wide. It is the member ($n = 2$) of the (n)-ITB family of related structures (3). The compositions of the neodymium bronzes will be given by the formula $(Nd,Ca)_xWO_3$ ($x \leq 0.1$), because microanalysis studies revealed that some crystal fragments contained a small amount of calcium due to reaction with the high-pressure chamber wall (1). In the Pr–W–O system ordered intergrowth tungsten bronzes, Pr_xWO_3, of (n)-ITB structure type were observed for $n = 2$, 3, and 4 and with a praseodymium content of $0.04 \leq x \leq 0.1$ (2). In both the (n)-ITB and the HTB structures, between 30 and 50% of the hexagonal tunnel sites are filled by (Nd,Ca) or Pr atoms.

It is known that rare earth tungsten bronzes, RE_xWO_3, synthesized by solid state reaction under ambient pressure conditions form perovskite tungsten bronzes (PTBs) with cubic unit cells ($a \approx 3.8$ Å) for RE = Ce–Lu and $x \approx 0.1$ (4,5). In the system Eu–W–O a tetragonal PTB bronze has been reported for low values of x ($x \approx 0.05$) (6). Recent HRTEM and microanalysis studies of bronze-type samples, La_xWO_3 and Nd_xWO_3 with $x \leq 0.3$, prepared in sealed evacuated silica tubes at $T \approx 1270$ K, revealed ordered, disordered, and twinned superstructures of PTB (7).

In view of the structural differences between rare earth tungsten bronzes synthesized under high-pressure (50 kbar) and under ambient pressure conditions we found it worthwhile to investigate a few samples prepared at $P \approx 30$ kbar. The present paper deals with X-ray powder diffraction and electron microscopy studies of these materials.

EXPERIMENTAL

Samples of starting compositions $La_{0.1}WO_3$ and Nd_xWO_3 with $x = 0.1$ and 0.2 were prepared by mixing appropriate amounts of RE_2O_3 (RE = La and Nd), WO_3, and W-metal powder in an agate mortar, both as dry powders and under acetone. The resulting mixtures were dried and pressed into pellets, which were wrapped up in

0022-4596/00 $35.00

TABLE 1
Sample Composition, Synthesis Temperature, Phase Identification from X-Ray Powder and ED Patterns, Unit Cell Parameters Refined from the X-Ray Data, ED–EDS Results and Occupation of the Hexagonal Tunnel Sites

Starting composition	T (K)	Unit cell dimensions			Phase	Unit cell content	RE_xWO_3		Occupancy, %
		a (Å)	b (Å)	c (Å)			x_{max}	x_{obs}	
$La_{0.1}WO_3$	1620	27.738(8)	7.3965(7)	3.8168(3)	(3)-ITB	$La_2W_{14}O_{42}$	0.14	0.04–0.07	30–50
		10.1212(8)	7.4037(7)	3.8151(3)	(2)-ITB	LaW_5O_{15}	0.2	0.07–0.08	35–40
		≈ 33.2 *	≈ 7.4 *	≈ 3.8 *	(1,2)-ITB[a]	$La_4W_{16}O_{48}$	0.25	—	
		7.4045(7)		3.7945(4)	HTB	LaW_3O_9	0.33	0.11–0.14	30–45
$La_{0.1}WO_3$	1320	7.4058(3)		3.7929(3)	HTB	LaW_3O_9	0.33	0.06–0.14	20–45
					≈ WO_3				
$Nd_{0.1}WO_3$	1570	10.093(1)	7.3798(7)	3.8162(6)	(2)-ITB	NdW_5O_{15}	0.2	0.07–0.1	35–50
					(3)-ITB[a]	$Nd_2W_{14}O_{42}$	0.14	0.03–0.07	20–50
		7.3906(4)		3.7938(4)	HTB	NdW_3O_9	0.33	0.10–0.12	30–40
		3.8148(2)			PTB	$NdWO_3$	1.0	0.10–0.11	≈ 10
$Nd_{0.2}WO_3$	1420	7.3911(2)		3.7914(3)	HTB	NdW_3O_9	0.33	0.08–0.15	25–45
					≈ WO_3				
Pr_xWO_3	1570				(4)-ITB[a]				
					(3)-ITB[a]				
		10.17	7.418	3.790	(2)-ITB				
		7.398		7.583	HTB				
$(Nd,Ca)_xWO_3$	1520	10.138	7.423	3.792	(2)-ITB				
		7.395		7.585	HTB				

Note. The cell parameters obtained from the ED study are marked *. Data from Ref. (2) (Pr_xWO_3) and Ref. (1) $(Nd,Ca)_xWO_3$ are included.
[a] Phases only observed by HRTEM.

tungsten foils to avoid chemical reaction between the samples and the surrounding high-pressure cell material. A description of the high-pressure equipment is given in Ref. (8). All samples were heat-treated under a pressure of $P = 30$ kbar. The applied pressure was stabilized after approximately 15 min. The sample was then heated to the desired temperature which was held for 5 to 7 min and then quenched to room temperature before the pressure was released. The starting compositions and the temperatures used are given in Table 1. A large number of synthesis experiments have shown that the chemical reaction is fast under the experimental conditions used and the heating times in the present study have thus been optimized.

All products were examined by X-ray powder diffraction, scanning electron microscopy (SEM), energy-dispersive X-ray spectroscopy (EDS analysis), and high-resolution transmission electron microscopy (HRTEM) methods. The X-ray powder patterns were taken in a Guinier–Hägg focusing camera with monochromatized Cu$K\alpha_1$ radiation and with Si as internal standard. The unit-cell parameters were refined from the X-ray powder data ($6^\circ < 2\Theta < 90^\circ$) with the program PIRUM, using least-squares methods (9).

The purity of the bulk samples was checked in a JEOL 820 scanning electron microscope, equipped with a LINK AN10000 EDS microanalysis system. The TEM specimens were prepared by crushing a small amount of the sample in an agate mortar, dispersing the fine powder in *n*-butanol, and finally putting a drop of the suspension on a holey carbon film supported by a Cu grid. Many crystal fragments on the Cu grid were analyzed in a JEOL 2000FXII transmission electron microscope, equipped with a LINK AN10000 EDS microanalysis system. Electron diffraction (ED) and microanalysis studies were performed on the same crystal fragment, to yield information about the structure type and RE/W content in at.%. The results are based on the WL, LaL, and NdL lines in the EDS spectra. The HRTEM images were taken in a JEOL 3010 TEM, operated at an accelerating voltage of 300 kV. The radius of the objective aperture used corresponded to 0.68 $Å^{-1}$ in reciprocal space. The structure models were drawn with the program ATOMS by Shape Software.

RESULTS

All samples were microcrystalline and had a dark blue color. They contained more than one phase, which could be seen both from the Guinier–Hägg photographs and from the EDS analysis of individual crystals in the scanning electron microscope. Some of the lines in the X-ray powder patterns could be identified as representing the hexagonal tungsten bronze structure RE_xWO_3, recently reported for $(Nd,Ca)_xWO_3$ and Pr_xWO_3 (1,2). The combined ED–EDS study of individual crystallites showed that a small amount of the starting material (≈ WO_3) still remained in the sam-

ples, although this was not always revealed by the Guinier–Hägg photographs.

(a) $La_{0.1}WO_3$, Synthesis Temperature $T = 1620$ K

The X-ray powder pattern of $La_{0.1}WO_3$ was quite complex and differed completely from that of the cubic perovskite tungsten bronze $RE_{\approx 0.1}WO_3$ and also from the X-ray patterns of the WO_3 modifications. However, it resembled to some extent the X-ray powder pattern previously taken of Pr_xWO_3 (2), thus indicating that the intergrowth tungsten bronze, (2)-ITB, could be present in the sample. This was later confirmed by the electron microscopy study.

Most of the ED patterns recorded from thin crystallites were identified as representing ordered crystals of (2)-ITB and (3)-ITB. The two characteristic ED patterns taken along the short crystal *c*-axes (3.8 Å) are illustrated in Fig. 1a and Fig. 1b, respectively. The patterns differ in the lattice spacings along a^* and in the absence or presence of a lattice centering. The latter can be seen in Fig. 1b. The lattice spacings correspond to *d* values of ≈ 10.1 and ≈ 13.9 Å, respectively, thus giving *a*-axis lengths of ≈ 10.1 Å ((2)-ITB)

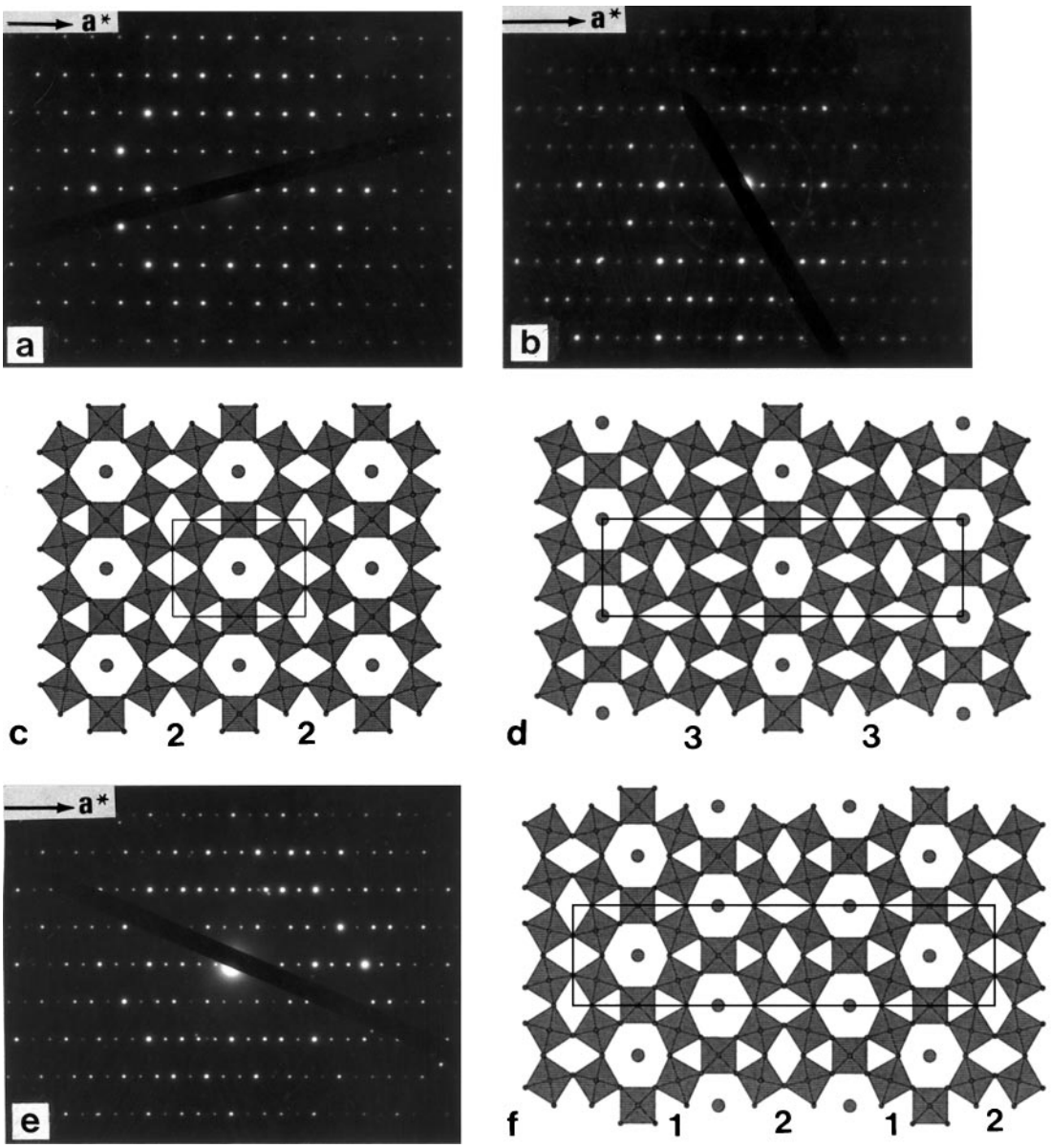

FIG. 1. ED patterns in [001] projection of (a) (2)-ITB and (b) (3)-ITB, and the corresponding crystal structures are shown in (c) (2)-ITB and (d) (3)-ITB. The ED pattern of a (1,2)-ITB crystal projected along [001]is given in (e) and the corresponding crystal structure of (1,2)-ITB in (f). The unit cells are outlined.

TABLE 2
A Part of the X-Ray Powder Data for $La_{0.1}WO_3$ Prepared at $T = 1620$ K and $P = 30$ kbar

			3-ITB				2-ITB				HTB			
Int. (%)	d obs. (Å)	2Θ obs.	2Θ calc.	h	k	l	2Θ calc.	h	k	l	2Θ calc.	h	k	l
0.82	7.3931	11.961	11.956	0	1	0	11.944	0	1	0				
0.68	7.1370	12.392	12.375	1	1	0								
5.47	6.4089	13.806									13.799	1	0	0
2.13	5.9681	14.832					14.813	1	1	0				
0.73	5.7728	15.336	15.325	3	1	0								
3.40	5.0539	17.534					17.511	2	0	0				
3.05	4.6206	19.193	19.170	6	0	0								
0.65	4.1791	21.243					21.249	2	1	0				
100.00	3.8164	23.289	23.288	0	0	1	23.297	0	0	1				
51.07	3.7976	23.406									23.425	0	0	1
27.25	3.7009	24.027	24.046	0	2	0	24.020	0	2	0	24.018	1	1	0
10.14	3.5737	24.895	24.898	2	2	0								
50.95	3.4701	25.651	25.655	8	0	0	25.602	1	2	0				
25.33	3.3711	26.417					26.397	3	0	0				
14.49	3.2643	27.299	27.305	4	2	0					27.287	1	0	1
36.28	3.2070	27.795									27.803	2	0	0
1.38	3.0688	29.075					29.063	3	1	0				
1.39	3.0461	29.296					29.293	2	0	1				
24.22	2.9877	29.882					29.881	2	2	0				
0.79	2.9445	30.331	30.336	6	0	1								
12.26	2.8882	30.936	30.933	6	2	0								
0.85	2.8184	31.723					31.736	2	1	1				
18.32	2.6577	33.696	33.721	0	2	1	33.709	0	2	1				
4.47	2.6097	34.335	34.351	2	2	1								
27.09	2.5704	34.877					34.887	1	2	1				
23.09	2.5284	35.475	35.448	8	2	0	35.491	3	0	1				
3.45	2.4923	36.006					35.988	3	2	0				
5.09	2.4821	36.160	36.186	4	2	1								
17.55	2.4491	36.664									36.665	2	0	1
0.96	2.3925	37.564					37.575	3	1	1				
15.23	2.3535	38.210					38.230	2	2	1				
7.42	2.3048	39.049	39.077	6	2	1								
1.07	2.2183	40.638	40.607	10	2	0	40.640	2	3	0				
0.54	2.1378	42.239									42.246	3	0	0
4.39	2.1096	42.833	42.847	8	2	1	42.852	4	0	1				
6.26	2.0884	43.289					43.277	4	2	0				
0.59	2.0423	44.317									44.311	2	1	1
1.89	2.0229	44.766					44.734	5	0	0				
0.56	1.9912	45.517					45.502	3	3	0				
3.76	1.9819	45.744	45.725	14	0	0								
1.42	1.9610	46.259	46.258	12	2	0								
9.54	1.9075	47.636	47.614	0	0	2	47.634	0	0	2				
2.98	1.8974	47.905									47.909	0	0	2
0.65	1.8618	48.880									48.865	3	0	1
24.20	1.8512	49.179					49.186	0	4	0	49.180	2	2	0
4.28	1.8328	49.704	49.705	2	4	0	49.721	4	2	1				

and ≈ 27.8 Å ((3)-ITB). Using the information from the ED patterns, a large number of lines in the X-ray powder pattern could be indexed as can be seen in Table 2 and the refined unit cell parameters of the two ITB bronzes are given in Table 1. Both the ED pattern (Fig. 1b) and the indexed X-ray powder pattern of the (3)-ITB phase show the absences of reflections ($hk0$) with $h + k = 2n + 1$. The structure models of (2)-ITB and (3)-ITB are shown in Fig. 1c and Fig. 1d, respectively. Both structures can be seen as built up by lamellar intergrowth of HTB and WO_3 slabs. They are the members $n = 2$ and $n = 3$ of the (n)-ITB structure family (3), as the HTB slabs are one hexagonal tunnel row wide and

the WO_3 slabs n octahedra across. Previously, only a few crystal fragments of the (3)-ITB structure type have been found for Pr_xWO_3 (2).

The ED pattern in Fig. 1e, taken along the 3.8 Å axis, resembles that recorded from a (3)-ITB fragment in Fig. 1b. Both patterns show lattice centering and approximately the same lattice spacing along b^*, but differ in the lattice spacing along a^*. The unit-cell parameters calculated from Fig. 1e are $a \approx 2 \times 16.6 \approx 33.2$ Å, $b \approx 7.4$ Å, and $c \approx 3.8$ Å (projection axis). These values clearly show that the ED pattern does not represent a member of the (n)-ITB family, as (4)-ITB will have a primitive unit cell with $a \approx 17.8$ Å and (5)-ITB will have a centered unit cell with $a \approx 2 \times 21.2 \approx 42.4$ Å. The pattern could be identified as yielded by the member $n = 2$ of the (1,n)-ITB family (3). The structure of (1,2)-ITB shown in Fig. 1f is built up of HTB slabs, two hexagonal tunnel rows wide, intergrown with WO_3 slabs two octahedra wide. It has previously been reported for a tin–tungsten bronze with the unit-cell dimensions $a \approx 33.24$, $b \approx 3.795$, and $c \approx 7.12$ Å (10).

The stoichiometric compositions of the ITB phases with all hexagonal tunnels fully occupied and the theoretical upper limit of x in the formula La_xWO_3 are given in Table 1. All ED patterns recorded of ITB crystallites showed sharp reflection spots, thus indicating well-ordered crystals. The EDS results given in Table 1 indicate that the hexagonal tunnels in the ITB structures are less than half-filled. This is in agreement with previous results obtained for the corresponding ITB structures of Pr_xWO_3 (2).

A typical HRTEM image of a well-ordered (2)-ITB crystal in [001] projection is shown in Fig. 2a. The image is taken close to Scherzer condition, which means that the black spots represent projected metal atoms. The micrograph clearly shows that the lanthanum content in the six-sided tunnels varies. Some tunnels in the thin part of the crystal seem to be almost empty, while others are more or less filled, but the La content x cannot be determined from the image. One type of local defect observed in a few (2)-ITB crystals is illustrated in Fig. 2b, with a hypothetical model given in Fig. 2c. The defect can be described as a fracture in the crystal parallel to the a-axis. The (2)-ITB regions on each side of the crack are mutually displaced by approximately one atom row, as can be seen in Fig. 2c. Such a defect will not give rise to any detectable change in composition of the fragment.

The low-magnification micrograph in Fig. 3 is taken from the (1,2)-ITB crystal, the ED pattern of which was given in Fig. 1e. Unfortunately, the crystal was too thick to give an atomic-resolution image. However, it is possible to see the arrangement of tunnels in the structure, as the white dots in the image represent the tunnel positions. The double hexagonal-tunnel rows are clearly revealed in the micrograph, thus confirming the structure model displayed in Fig. 1f.

In addition to the ITB phases above, a few crystallites yielded ED patterns that could be identified as due to an HTB fragment. There was no sign of diffuse streaking of the spots or superstructure reflections in the patterns, which means that the examined crystals were fairly well-ordered. The remaining lines in the X-ray powder pattern (Table 2) could be indexed and refined with the hexagonal unit cell given in Table 1. According to the EDS results detailed in Table 1, between 30 and 45% of the hexagonal-tunnel sites in the HTB structure are occupied by randomly distributed lanthanum atoms.

(b) $La_{0.1}WO_3$, Synthesis Temperature $T = 1320$ K

The X-ray powder pattern of the low-temperature $La_{0.1}WO_3$ sample did not show any lines characteristic of ITB. This was also confirmed by the transmission electron microscopy study. No ED patterns corresponding to any of the three ITB phases, (2)-ITB, (3)-ITB, and (1,2)-ITB, have been observed so far.

The X-ray and electron microscopy results showed that HTB and $WO_{\approx 3}$ were the dominating phases in the sample. The unit cell parameters of HTB refined from the X-ray data are given in Table 1. These values are very similar to those obtained for HTB from the high-temperature sample above. According to the combined ED–EDS studies of thin crystallites, the La content of the HTB crystals varied between the different fragments (see Table 1), whereas the $WO_{\approx 3}$ crystallites did not contain any detectable amounts of lanthanum. The analyzed HTB crystals seemed to be well-ordered, as the ED patterns did not show any streaking of the reflection spots. The EDS results indicate that approximately 1/3 of the hexagonal tunnel sites are occupied by La atoms.

(c) $Nd_{0.1}WO_3$, Synthesis Temperature $T = 1570$ K

HRTEM studies revealed the presence of ordered crystals of (2)-ITB, (3)-ITB, and HTB in the high-temperature sample of $Nd_{0.1}WO_3$. Figure 4 is taken from a well-ordered fragment of (3)-ITB. The HTB slabs, one hexagonal tunnel row wide, and the WO_3 slabs, three octahedra wide, can be clearly seen in the image. According to the EDS results (Table 1), approximately 1/3 of the hexagonal-tunnel sites in the (3)-ITB structure are occupied by Nd atoms, but the variation in tunnel occupancy cannot be easily seen in the thin part of the image. Previous results obtained for the alkali tungsten bronzes (11) have shown that the variation in tunnel occupancy cannot be seen in the thicker part of the crystal.

Different occupancy of the hexagonal-tunnel sites was also observed in the HTB crystals. The HRTEM image in Fig. 5a shows randomly distributed large white dots, which represent empty or almost empty hexagonal tunnels in the HTB structure shown in Fig. 5b. According to the EDS

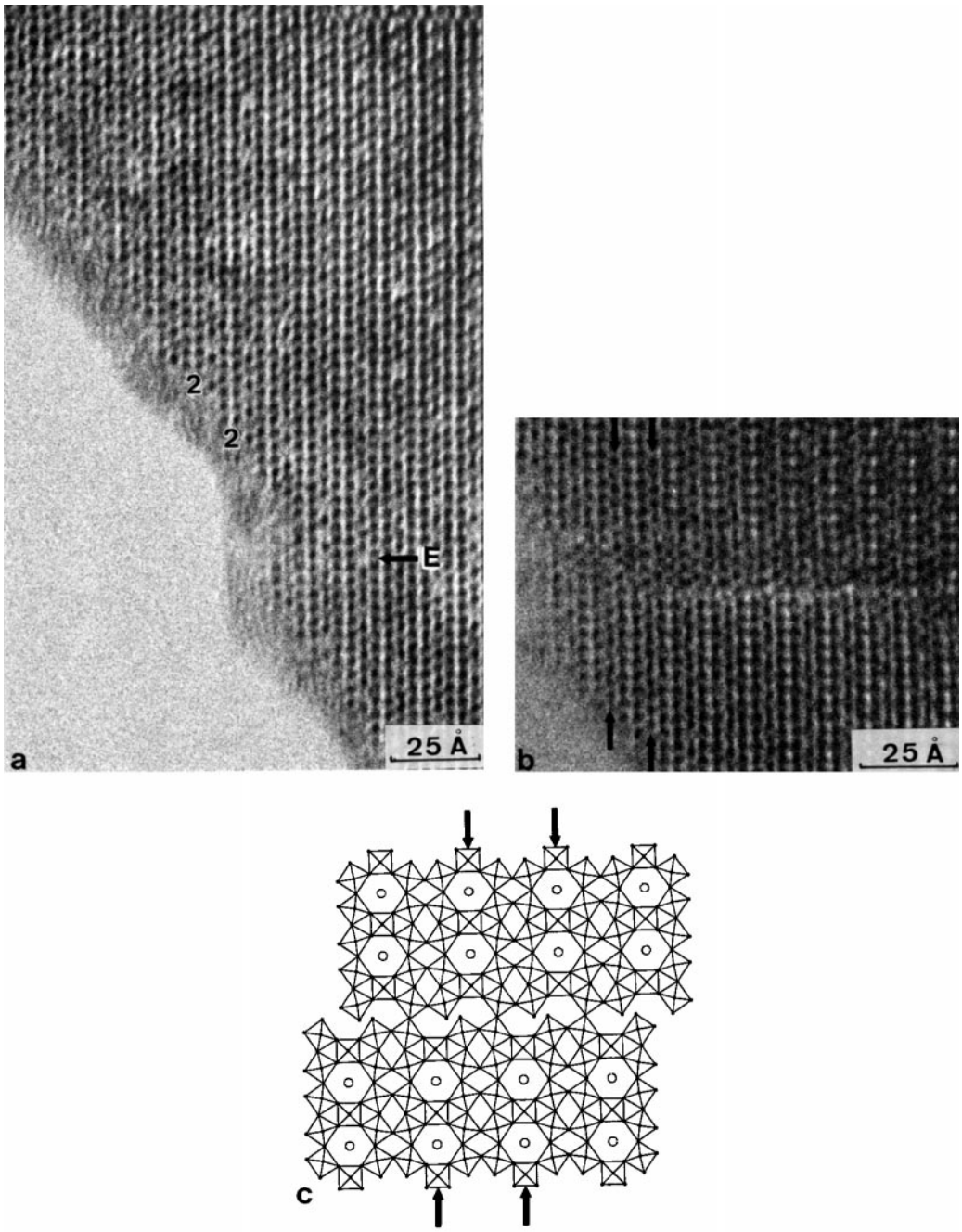

FIG. 2. (a) HRTEM images of a (2)-ITB crystal projected along [001]. An empty or almost empty tunnel is marked with E. (b) HRTEM image of a local defect in a (2)-ITB crystal and the corresponding hypothetical model is illustrated in (c). The arrows show the hexagonal tunnel rows.

results in Table 1, less than 40% of the hexagonal-tunnel sites are occupied by neodymium. The results are in fairly good agreement with those reported above for the La-containing ITB and HTB crystals from the high-temperature sample of $La_{0.1}WO_3$.

An example of a defect-rich essentially (2)-ITB crystal is illustrated in Fig. 6. The ED pattern inserted in the corresponding HRTEM image in Fig. 6a shows streaking along a^*, indicating WO_3 and HTB slabs of different widths in the (2)-ITB structure. This was also confirmed by HRTEM image, which shows HTB slabs, two hexagonal-tunnel rows wide, and WO_3 slabs, three octahedra across, intergrown with (2)-ITB. The region marked in the micrograph illustrates a local intergrowth of thin lamellas of (1,3)-ITB in the (2)-ITB phase. The corresponding structure model is given in Fig. 6b. No ordered fragment of the (1,3)-ITB structure

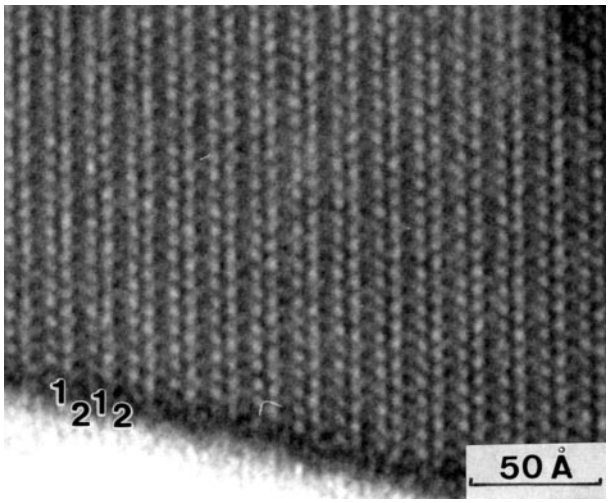

FIG. 3. Low-magnification micrograph of a thick (1,2)-ITB crystal. The white dots represent the hexagonal tunnels, and the sequence of octahedra is marked.

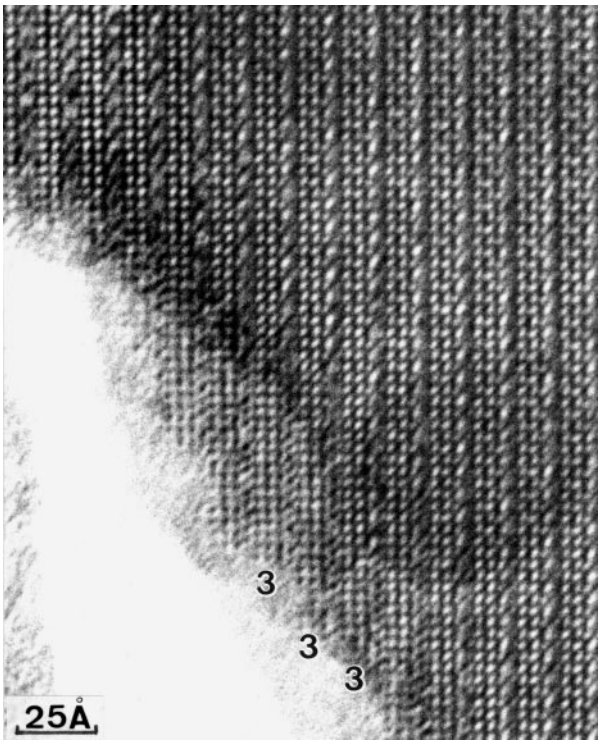

FIG. 4. HRTEM image of a (3)-ITB crystal projected along [001]. The three octahedra separating the hexagonal-tunnel rows can be seen in the thinnest part of the crystal.

has been found so far in the Nd-bronzes, but ordered (1,3)-ITB crystals were observed in mixed W–Mo ITB bronzes containing potassium or cesium (12,13).

The electron microscopy studies also revealed some crystal fragments of PTB type structure in the high-temperature sample of $Nd_{0.1}WO_3$. A typical example is shown in Fig. 7. The ED pattern exhibits a cubic lattice with $d \approx 3.8$ Å, and a square arrangement of black spots can be seen in the corresponding HRTEM image, representing the projected framework of corner-sharing WO_6 octahedra in the PTB structure. The image also clearly shows that some of the square tunnels (*A* sites in PTB) are partly occupied by neodymium atoms. The ED–EDS studies of the PTB fragments gave an Nd content of about 8 at.%, thus corresponding to an average composition of $Nd_{\approx 0.1}WO_3$.

Based on the electron diffraction results, the X-ray powder pattern could be indexed and the unit cell dimensions of (2)-ITB, HTB, and PTB refined from the X-ray data are given in Table 1. The 2Θ region ($10^\circ < 2\Theta < 40^\circ$) in the X-ray powder patterns of the high-temperature samples of $La_{0.1}WO_3$ and $Nd_{0.1}WO_3$ are illustrated in Fig. 8. Peaks characteristic of the (2)-ITB and HTB compounds are present in both patterns whereas peaks from the (3)-ITB phase were only seen in the X-ray photograph of $La_{0.1}WO_3$. On the other hand, the peak at $2\Theta = 33.186^\circ$ which is characteristic of the PTB structure can only be observed in the X-ray pattern of $Nd_{0.1}WO_3$.

(d) $Nd_{0.2}WO_3$, Synthesis Temperature $T = 1420$ K

The X-ray powder pattern of $Nd_{0.2}WO_3$ resembled that taken of the low-temperature sample of $La_{0.1}WO_3$. Many of the lines in the X-ray pattern could be indexed with an HTB cell, and the refined unit-cell parameters are given in Table 1. The ED–EDS study revealed fragments of HTB and WO_3 structure type. The EDS results showed the Nd content to vary considerably among the HTB fragments. Despite the high Nd content in the starting material, only between 25 and 45% of the hexagonal tunnel sites seemed to be occupied by Nd atoms. The $WO_{\approx 3}$ crystals were pure, as no peaks characteristic of Nd could be seen in the EDS records. Most of the remaining weak lines in the X-ray pattern could also be assigned to WO_3. No presence of ITB or PTB crystals could be found in this sample, either from the ED–EDS study or from the X-ray powder pattern.

DISCUSSION

The results presented in Table 1 show that RE_xWO_3 bronzes (RE = La or Nd) of HTB structure type are formed in all samples prepared at $P = 30$ kbar, whereas ITB-type bronzes are only formed at high temperatures. It is interesting to note that similar high-temperature conditions ($T = 1520$–1570 K) were used in the solid-state syntheses of $(Nd,Ca)_xWO_3$ and Pr_xWO_3 bronzes with (*n*)-ITB structures at $P = 50$ kbar (1,2). Our results clearly show that ITB-related phases can be formed by solid state reaction above $T \approx 1500$ K and $P = 30$–50 kbar and that the temperature is a crucial factor in the formation of ITB-type structures.

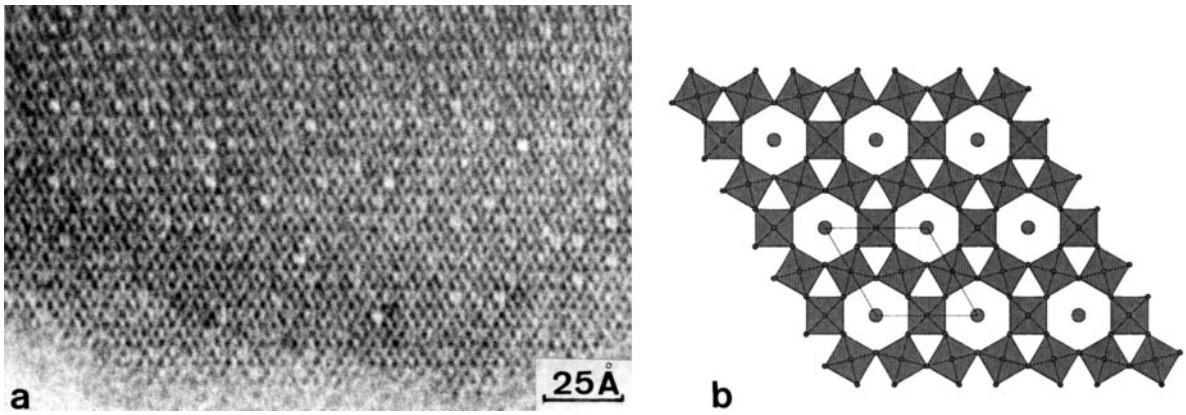

FIG. 5. (a) Low-magnification micrograph of an HTB crystal projected along [001]. The large white dots represent empty or almost empty tunnels. (b) Crystal structure of HTB with the unit cell outlined.

This is in agreement with previous results obtained on the alkali tungsten bronzes, A_xWO_3 with A = K, Rb, and Cs, prepared by solid state reaction and ambient pressure conditions (14). In the phase analysis study Hussain (14) showed that ITB-type structures were formed at $T > 1070$ K. He observed phase mixtures of WO_3 and ITB for low values of x and phase mixtures of ITB and HTB in the composition region $0.11 < x < 0.2$. In analogy with our results, Hussain also observed two-phase mixtures of WO_3 and HTB in samples prepared at lower temperatures. TEM studies of the

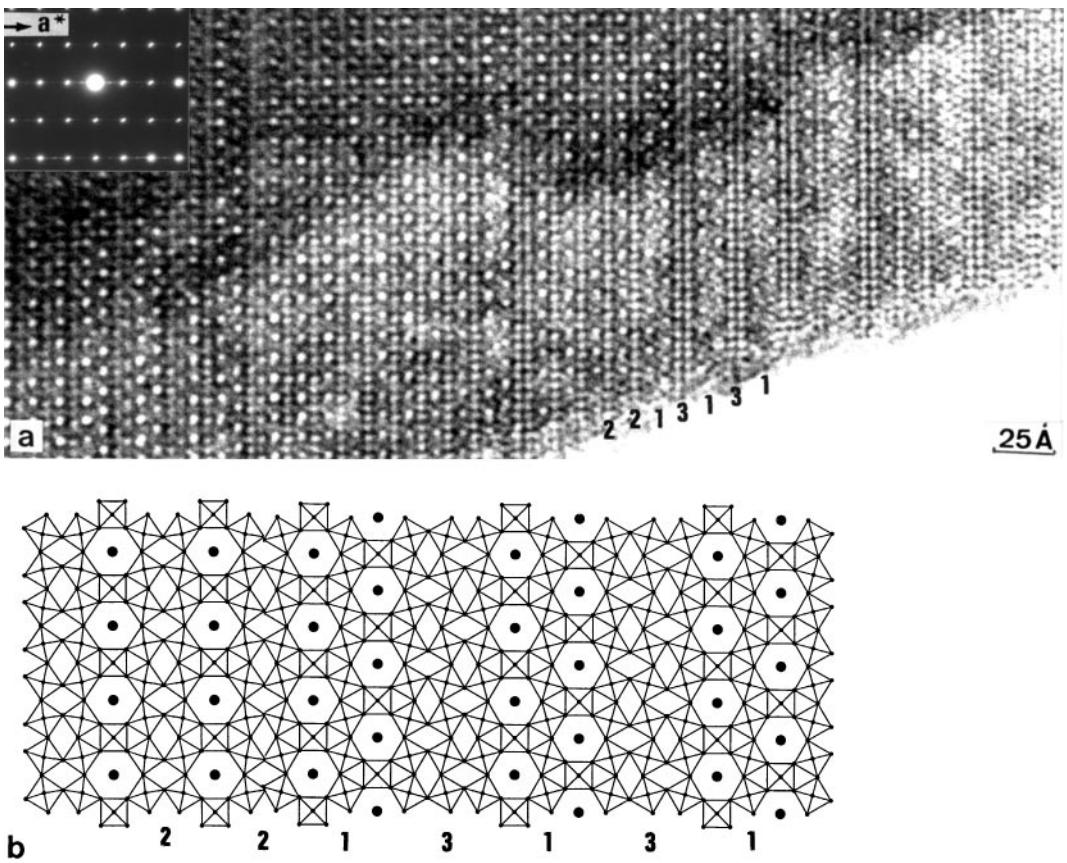

FIG. 6. (a) HRTEM image of a defect-rich region of a (2)-ITB crystal showing intergrowth of (1,3)-ITB. The inserted ED pattern shows considerable streaking along a^*. (b) Hypothetical model of the intergrowth of the (2)-ITB and the (1,3)-ITB structures.

FIG. 7. HRTEM image of a PTB crystal projected along [0 0 1]. Partial occupancy of the tunnels in the perovskite lattice can be seen, especially in the thinner region of the crystal.

Cs_xWO_3 samples revealed (n)-ITB type structures ($n > 6$) in samples with $x = 0.03$ and 0.05, and crystals of (1,n)-ITB type ($n > 6$) in samples with $x \geq 0.05$ (15).

In the present study almost all ITB crystals were of (n)-ITB structure type with $n = 2$ or $n = 3$. Only a few ordered crystals of (1,2)-ITB were seen in the $La_{0.1}WO_3$ sample. It is noteworthy that both the (2)-ITB and (3)-ITB phases could be identified from the X-ray powder pattern of the sample prepared at the highest temperature ($T = 1620$ K), whereas only the (2)-ITB phase was revealed by the X-ray patterns of the samples prepared at $T < 1620$ K. Our results indicate that higher synthesis temperature favors the formation of ITB members with higher n values, which means that the thickness of the WO_3 slabs increases with temperature, despite the high-pressure conditions. The same relationship between temperature and ITB-phases formed has previously been found for the alkali (1,n)-ITB structures (16).

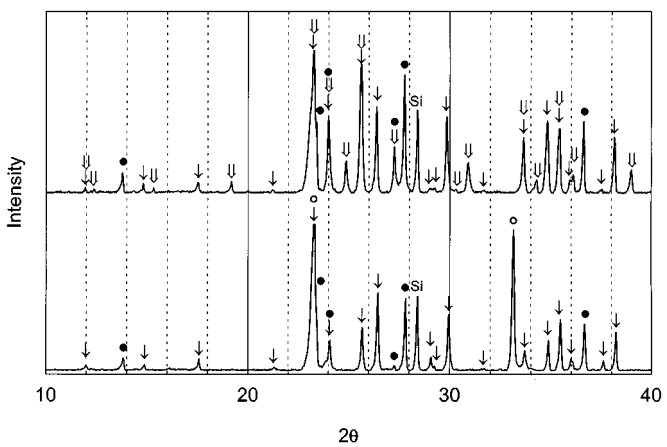

FIG. 8. A part of the X-ray powder diffraction patterns ($10° < 2\Theta < 40°$) of the high-temperature samples of $La_{0.1}WO_3$ (top) and $Nd_{0.1}WO_3$ (bottom). The peaks characteristic of (3)-ITB (double arrow), (2)-ITB (single arrow), HTB (black spot), and PTB (unfilled circle) are marked.

In the general formula RE_xWO_3 the rare earth content x is associated both with the number of hexagonal tunnels in relation to the number of tungsten atoms in the bronze type structure and with the occupancy of the hexagonal tunnel sites. The unit-cell content calculated from the bronze type structure with all hexagonal tunnel sites filled with RE atoms is given in Table 1 together with the x_{max} value. As can be seen from Table 1, the maximum RE content, x_{max}, increases when the thickness of the WO_3 slab decreases. It also increases with increasing number of hexagonal-tunnel rows in the structure. By combined ED–EDS investigations of individual crystallites, the observed x values given in Table 1 were obtained, and the occupancy of the hexagonal-tunnel sites was calculated. The main EDS results from ITB crystallites show that between 30 and 50% of the hexagonal-tunnel sites are filled with RE atoms. This is in agreement with previous observations on the Pr_xWO_3 and $(Nd,Ca)_xWO_3$ bronzes (1,2). In the present study, however, we have not seen any impurity peaks from Ca in the EDS records. A single-crystal X-ray structure determination of a cesium (1,7)-ITB-type crystal indicated that the hexagonal-tunnel sites were filled by cesium to 62% (17). Isotypic tungsten bronzes, M_xWO_3, of (n)-ITB structure type have been reported for M = Ba, Sn, Sb, and Bi (18–21). However, no microanalysis studies have been performed on these compounds.

The hexagonal tungsten bronze structure, A_xWO_3 (A = alkali), is formed for $0.19 < x < 0.33$, which means that at least 60% of the tunnel sites are occupied by alkali metal ions (14). In the present study the HTB-structure is formed for $0.06 \leq x \leq 0.15$ in the low-temperature region and for $0.10 \leq x \leq 0.14$ at higher temperatures. The filling of the tunnels might thus increase slightly with temperature.

It is noteworthy that the average value of the tunnel occupancy ($x = 0.11$) is approximately 1/3 of $x_{max} = 0.33$. This probably reflects the differences in valence state between *RE* (+3) and alkali (+1) ions.

The fact that a cubic PTB bronze of composition $Nd_{\approx 0.1}WO_3$ is formed under high-pressure and high-temperature conditions is noteworthy. The observed composition is also the same as that previously reported for the $RE_{0.1}WO_3$ bronzes prepared under high-temperature and ambient-pressure conditions (4). The lattice parameter of $Nd_{0.1}WO_3$ given in Table 1 is similar to that ($a = 3.822$ Å) previously reported by Ostertag (4). In the PTB bronze structure the network of corner-sharing WO_6 octahedra is regular, and the Nd atoms which stabilize the structure are randomly distributed in the square tunnels. In the ITB-type structures, however, the WO_3 network is heavily distorted because the octahedra are tilted around an axis normal to intergrowth direction, in order to fit perfectly to the HTB-type slabs. According to the HRTEM results the *RE* atoms enter the six-sided tunnels to stabilize the ITB structure. We have no indications so far from the HRTEM images that the *RE* atoms are located in the deformed four-sided tunnels in the WO_3 slabs.

The results presented above illustrate that a combination of electron microscopy and X-ray powder diffraction techniques is very useful in exploring the formation conditions of the lanthanum and neodymium tungsten bronzes at a pressure of 30 kbar. The different bronze type structures were identified by the combined ED–EDS study and the local crystal structures determined from HRTEM images. By using the information from the electron microscopy study the X-ray powder patterns could be successfully indexed and the unit-cell dimensions of lanthanum and neodymium tungsten bronzes determined and refined. Further experiments are under way to establish the formation conditions of rare earth tungsten bronzes at pressures of 50–80 kbar.

ACKNOWLEDGMENTS

We thank Mrs. Jaroslava Östberg for technical assistance with the photographic work. The research described here was partly made possible by a Visiting Scientist Grant from the Royal Swedish Academy of Sciences through its Nobel Institute for Chemistry. This support is gratefully acknowledged. The present study forms part of a research project financially supported by the Swedish Natural Science Research Council.

REFERENCES

1. N. D. Zakharov, Z. Liliental-Weber, V. P. Filonenko, I. P. Zibrov, and M. Sundberg, *Mater. Res. Bull.* **31,** 373 (1996).
2. N. D. Zakharov, P. Werner, I. P. Zibrov, V. P. Filonenko, and M. Sundberg, *J. Solid State Chem.* **147,** 536 (1999).
3. A. Hussain and L. Kihlborg, *Acta Cryst. Sect. A* **32,** 551 (1976).
4. W. Ostertag, *Inorg. Chem.* **5,** 758 (1966).
5. I. N. Belyaev and L. A. Voropanova, *Zhur. Neorg. Khi.* **21,** 3107 (1976).
6. C. S. Dimbylow, I. J. McColm, C. M. P. Barton, N. N. Greenwood, and G. E. Turner, *J. Solid State Chem.* **10,** 128 (1974).
7. C. Grenthe and M. Sundberg, manuscript in preparation.
8. I. P. Zibrov, V. P. Filonenko, P.-E. Werner, B.-O. Marinder, and M. Sundberg, *J. Solid State Chem.* **141,** 205 (1998).
9. P.-E. Werner, *Arkiv Kemi.* **31,** 513 (1969).
10. R. Steadman, R. J. D. Tilley, and I. J. McColm, *J. Solid State Chem.* **4,** 199 (1972).
11. L. Kihlborg and M. Sundberg, *Acta Cryst. Sect. A* **44,** 798 (1988)
12. H. Blomqvist and M. Sundberg, "Proc. 50th SCANDEM Meeting," p.145, Finland, 1998.
13. L. Kihlborg, L.-J. Norrby, and M. Sundberg, "Proc. 49th SCANDEM Meeting," p. 102, Göteborg, Sweden, 1997.
14. A. Hussain, *Acta Chem. Scand. A* **32,** 479 (1978).
15. L. Kihlborg, *Chem. Scr.* **14,** 187 (1978–79).
16. L. Kihlborg, M. Fernandez, Y. Laligant, and M. Sundberg, *Chem. Scr.* **28,** 71 (1988).
17. A. Hussain, *Chem. Scr.* **11,** 224 (1977).
18. T. Ekström and R. J. D. Tilley, *J. Solid State Chem.* **28,** 259 (1979).
19. T. Ekström, M. Parmentier, and R. J. D. Tilley, *J. Solid State Chem.* **37,** 24 (1981).
20. T. Ekström, M. Parmentier, and R. J. D. Tilley, *J. Solid State Chem.* **34,** 397 (1980).
21. D. A. Jefferson, M. K. Uppal, D. J. Smith, J. Gopalakrishnan, A. Ramanan, and C. N. R. Rao, *Mater. Res. Bull.* **19,** 535 (1984).